

MDAESF: Cine MRI Reconstruction Based on Motion-Guided Deformable Alignment and Efficient Spatiotemporal Self-Attention Fusion^{*}

Xiaoxiang Han¹[0000–0002–1946–2067], Yiman Liu^{2,3}[0000–0002–4115–8440], Yuanjie Lin¹, Naiyue Xu¹, Keyan Chen¹, Weikun Zhang¹, and Qiaohong Liu⁴(✉)

¹ School of Health Sciences and Engineering, University of Shanghai for Science and Technology, Shanghai 200093, China

{gtlinyer, linyuanjie0312, xunaiyue21, albertchendev, zwk7799}@163.com

² Department of Pediatric Cardiology, Shanghai Children’s Medical Center, School of Medicine, Shanghai Jiao Tong University, Shanghai 200127, China
LiuyimanSCMC@163.com

³ Shanghai Key Laboratory of Multidimensional Information Processing, School of Communication & Electronic Engineering, East China Normal University, Shanghai 200241, China

⁴ School of Medical Instruments, Shanghai University of Medicine and Health Sciences, Shanghai 201318, China
hq11qh@163.com

Abstract. Cine MRI can jointly obtain the continuous influence of the anatomical structure and physiological and pathological mechanisms of organs in the two dimensions of time domain and space domain. Compared with ordinary two-dimensional static MRI images, the information in the time dimension of cine MRI contains many important information. But the information in the temporal dimension is not well utilized in past methods. To make full use of spatiotemporal information and reduce the influence of artifacts, this paper proposes a cine MRI reconstruction model based on second-order bidirectional propagation, motion-guided deformable alignment, and efficient spatiotemporal self-attention fusion. Compared to other advanced methods, our proposed method achieved better image reconstruction quality in terms of peak signal-to-noise ratio (PSNR) and structural similarity index (SSIM) metrics as well as visual effects. The source code will be made available on <https://github.com/GtLinyer/MDAESF>.

Keywords: Deep Learning · Cine MRI · Reconstruction.

1 Introduction

Magnetic resonance imaging (MRI) is a widely used diagnostic tool in clinical settings, offering advantages such as non-invasiveness, absence of ionizing radiation, and multiple parameters. However, due to physiological and hardware

^{*} This research was partially supported by the National Natural Science Foundation of China (Project No. 61801288).

limitations, it tends to be slower than other imaging methods. As an important component of MRI technology, cine MRI enables continuous visualization of the anatomy and physiological and pathological mechanisms of organs in both temporal and spatial dimensions. Compared to regular static 2D MRI images, cine MRI’s temporal dimension contains many crucial details. Therefore, it has a wide range of applications in imaging the heart, vessels, and diagnosing cardiovascular diseases. However, cine MRI requires a larger amount of data collection and higher imaging time demands. Therefore, improving reconstruction algorithms is of great significance for the widespread use of cine MRI technology.

Collecting fewer k-space data during magnetic resonance imaging is the mainstream approach for MRI acceleration. However, due to violating the Nyquist theorem, directly performing Fourier inverse transformation on zero-filled and undersampled k-space data will result in images with aliasing artifacts. In the past, methods for recovering fully sampled MRI signals included partial Fourier transform [17], parallel imaging (PI) [9], compressed sensing (CS) [16], low-rank matrix completion [2], and manifold learning [18]. However, with the development of deep learning, reconstruction methods based on deep learning have surpassed the aforementioned methods. In 2016, Wang et al. [24] were the first to introduce deep learning into MRI reconstruction tasks. They used convolutional neural networks to establish a mapping relationship between a large number of undersampled images and fully sampled images, and then, during prediction, only inputted the undersampled images to obtain high-quality reconstructed images. Since then, numerous 2D MRI reconstruction algorithms based on deep learning have emerged [14,31,29,10,20].

Although great progress has been made in static MRI reconstruction, only a few studies have applied deep learning to cine (dynamic) reconstruction. Chlemper et al. [6] normalized the temporal correlation between different frames by introducing a Data Sharing (DS) layer into the 2D reconstruction model. Qin et al. [19] proposed CRNN, which uses convolutional recurrent neural networks to handle dynamic signals and utilizes bidirectional recurrent hidden connections across time sequences to learn spatiotemporal correlations. Sarasaen et al. [21] fine-tuned the network using static high-resolution MRI as prior knowledge. In addition, there are also some unsupervised methods [28,7,30]. Since motion information is an important prior in cine MRI, some studies [22,11] have improved cine MRI reconstruction by utilizing motion information.

2 Methods

2.1 Problem statement

Dynamical magnetic resonance reconstruction is formally an optimization problem, where a set of undersampled k-space data $\{y_f\}_{f \in [F]}$ from several frames of a given slice is used to predict $\{\theta\}$ from $\{y_f\}$ through a deep neural network.

$$\theta^* = \underset{\theta}{\operatorname{argmin}} \sum_{f=1}^F \frac{1}{2} \|F_u(\theta) - f_y\|_2^2 + \lambda R(\theta) \quad (1)$$

The first fidelity term $\|F_u(\theta) - f_y\|$ is used to ensure data consistency by constraining the reconstructed image θ to be close to the input value y_f . The operator $F_u(\cdot)$ transforms the image domain θ into the frequency domain and then performs undersampling. The second term $F_u(\cdot)$ is a regularization function that depends on prior knowledge of the input y_f . λ is a weighting factor. In the proposed method, motion information is an important prior knowledge.

2.2 Motion-guided deformable alignment

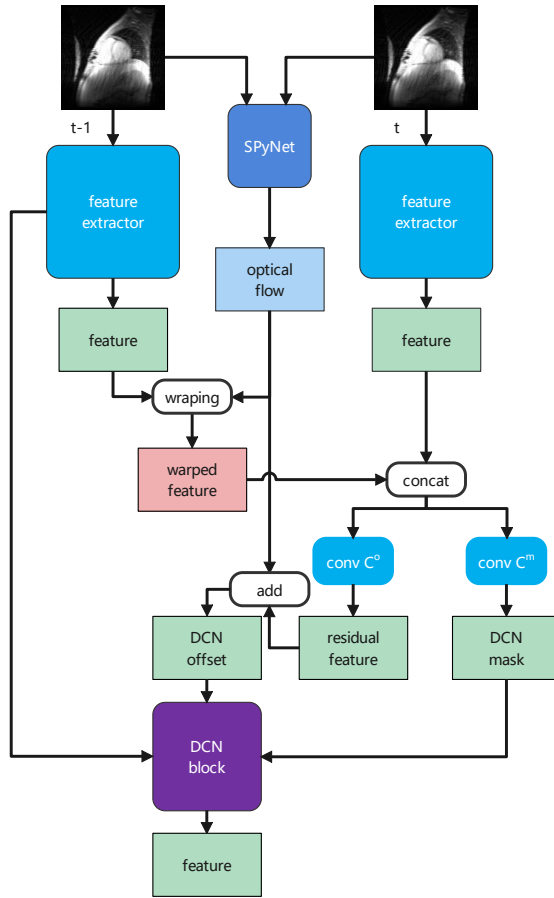


Fig. 1. Motion-guided deformable alignment module.

Deformable convolution has been applied to video super-resolution reconstruction [23], in which 2D displacements are added to the lattice sampling positions of standard convolution rules, allowing the sampling grid to deform freely. Since the displacement here needs to be learned from the previous layer features through another convolution layer, the deformation is local, dense, and adaptive to the input features [8]. However, DCN is difficult to train and the training process is unstable, and it may even cause offset overflow [4]. Therefore, we propose to use motion information to guide the learning of offsets in DCN. Usually, motion information can be obtained through optical flow estimation. However, traditional optical flow calculation requires a large amount of computation, so we use pre-trained SPyNet for optical flow estimation. The structure of the alignment module is shown in Fig. 1.

To make use of alignment features from further in the past or future, we introduce second-order grid propagation, where the current state not only receives hidden states from adjacent grid points, but also from points further away, as shown in Fig. 2. This approach improves the flow of

information in the network by introducing second-order Markovian properties, allowing for additional spatial positional features to be obtained during frame alignment [5].

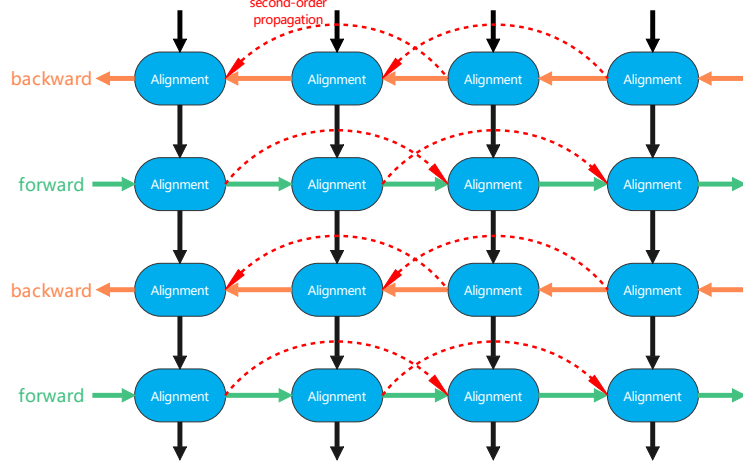


Fig. 2. Second-order grid propagation.

The expression of each grid point in the forward propagation process is as follows:

$$s_{i \rightarrow i-1}, s_{i \rightarrow i-2} = \mathcal{M}(x_i, x_{i-1}), \mathcal{M}(x_i, x_{i-2}) \quad (2)$$

$$\hat{f}_i^j = \mathcal{A} \langle g_i, f_{i-1}^j, f_{i-2}^j, s_{i \rightarrow i-1}, s_{i \rightarrow i-2} \rangle \quad (3)$$

In the equations above, x_i represents the input image at time step i . g_i represents the feature map obtained by extracting features from the input image at time step i . f_i^j represents the aligned and corrected feature map at time step i for the j th branch. When $j=0$, f_i^0 is equal to g_i . \hat{f}_i^j represents the feature map after motion-guided deformable alignment, which contains all the alignment information from the previous time steps $i-1$ and $i-2$. $s_{i \rightarrow i-1}$ and $s_{i \rightarrow i-2}$ represent the optical flow between frame i and frames $i-1$ and $i-2$, respectively. $\mathcal{M}(\cdot)$ denotes motion estimation, which is performed using pre-trained SPyNet for optical flow estimation.

Next, the aligned feature maps from the backward branch and the aligned feature maps from the forward branch are concatenated, and then sent to the feature correction module for improvement, with the specific expression as follows:

$$f_i^j = \hat{f}_i^j + \mathcal{Res} \langle \mathcal{Cat}(f_{i-1}^j, \hat{f}_i^j) \rangle \quad (4)$$

where $\mathcal{Cat}(\cdot, \cdot)$ represents concatenation and $\mathcal{Res}(\cdot)$ represents a stacked residual block.

The alignment operation under the second-order propagation is as follows, where $\mathcal{W}(\cdot, \cdot)$ represents pre-alignment:

$$\bar{f}_{i-1} = \mathcal{W}(f_{i-1}, s_{i \rightarrow i-1}) \quad (5)$$

$$\bar{f}_{i-2} = \mathcal{W}(f_{i-2}, s_{i \rightarrow i-2}) \quad (6)$$

Then, the results of alignment using optical flow \bar{f}_{i-1} , \bar{f}_{i-2} and optical flow $s_{i \rightarrow i-1}$, $s_{i \rightarrow i-2}$ are used to guide the learning of offsets and modulated scalars in DCN, by learning 2 offsets and modulation masks by merging 3 frames.

$$o_{i \rightarrow i-p} = s_{i \rightarrow i-p} + \mathcal{C}^o \langle \text{Cat}(g_i, \bar{f}_{i-1}, \bar{f}_{i-2}) \rangle \quad (7)$$

$$m_{i \rightarrow i-p} = \text{Sigmoid} \langle \mathcal{C}^m \langle \text{Cat}(g_i, \bar{f}_{i-1}, \bar{f}_{i-2}) \rangle \rangle \quad (8)$$

where $\mathcal{C}^o \langle \cdot \rangle$ and $\mathcal{C}^m \langle \cdot \rangle$ are stacks of convolutional neural network layers, and $p=1,2$.

Next, the learned offsets and modulation masks are merged to generate the final offsets (o_i) and modulation masks (m_i) used for DCN.

$$o_i = \text{Cat}(o_{i \rightarrow i-1}, o_{i \rightarrow i-2}) \quad (9)$$

$$m_i = \text{Cat}(m_{i \rightarrow i-1}, m_{i \rightarrow i-2}) \quad (10)$$

$$\bar{f}_i = \text{DCN}(\text{Cat}(f_{i-1}, f_{i-2}); o_i, m_i) \quad (11)$$

2.3 Efficient spatiotemporal self-attention fusion

In cine magnetic resonance imaging, both inter-frame and intra-frame correlation are important, but with different degrees of importance for different frames. On the one hand, there may be artifacts such as ghosting and blurring within a frame. In addition, if the alignment of adjacent frames is inaccurate or imprecise, then when the frames are fused, there will be differences in the content of the frames, which is equivalent to blurring and will affect the subsequent reconstruction.

To solve this problem, we introduce attention mechanisms both in time and space. This allows the model to ignore less useful feature information and focus more on the feature information that is beneficial for reconstruction. The proposed efficient spatiotemporal self-attention fusion module includes two parts: temporal attention and spatial attention, as shown in Fig. 3.

The purpose of temporal attention is to calculate the similarity between the current frame and the reference frame [26]. First, convolution is performed, then the similarity between each frame and the reference frame is calculated, and finally, the attention weight is applied to the input feature map pointwise. The calculation method is as follows:

$$w(F_{t+i}, F_t) = \text{Sigmoid}(\phi(F_{t+i})^T \varphi(F_t)) \quad (12)$$

where w represents the attention weight, $\phi(\cdot)$ and $\varphi(\cdot)$ represent convolution operations, F_t represents the feature map at time t , and F_{t+i} represents the reference feature map.

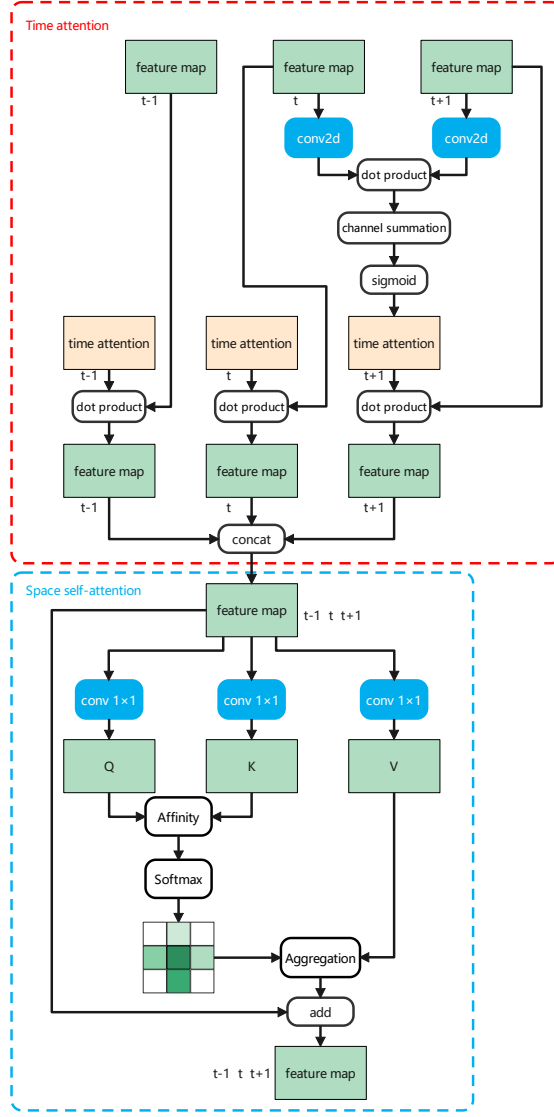


Fig. 3. Efficient spatiotemporal self-attention fusion module.

feature vector at position u in the feature map Q . $\Omega_u \in \mathbb{R}^{(H+W-1) \times C'}$ represents the feature vectors extracted from K that are in the same row or column as position u , and $\Omega_{i,u} \in \mathbb{R}^{C'}$ denotes the i -th element of Ω_u . $d_{i,u} \in D$ represents the correlation between the feature \mathcal{Q}_u and $\Omega_{i,u}$, $i = [1, \dots, |\Omega_u|]$, $D \in \mathbb{R}^{(H+W-1) \times W \times H}$.

After the above calculations, the obtained feature map is subjected to a Softmax operation to obtain an attention map A . The purpose of the Softmax operation is to normalize the position-related feature map, making the contribu-

As MRI images are more sparse and have more redundancy than natural images, we believe it is unnecessary to calculate self-attention for each pixel. The proposed method includes a spatial attention mechanism called the Criss-Cross Attention [12], which is an efficient form of self-attention. Its GPU resource consumption is only 1/11 of the Non Local [25] module, and it reduces floating point computation by 85% compared to the Non Local module.

First, the input feature map H goes through three 1×1 convolutional operations to generate Q , K , and V feature maps. The size of the input feature map is $(C \times W \times H)$. The channel numbers of Q and K are reduced to reduce computation, and their size is $(C' \times W \times H)$. The size of V is the same as the input feature map. Then, the Affinity operation is performed to obtain the relationship between each pixel in a $(W \times H)$ feature map and the pixels in the same row and column. Its calculation method is as follows:

$$d_{i,u} = \mathcal{Q}_u \Omega_{i,u}^T \quad (13)$$

$\mathcal{Q}_u \in \mathbb{R}^{C'}$ represents the feature vector at position u in the feature map Q . $\Omega_u \in \mathbb{R}^{(H+W-1) \times C'}$ represents the feature vectors extracted from K that are in the same row or column as position u , and $\Omega_{i,u} \in \mathbb{R}^{C'}$ denotes the i -th element of Ω_u . $d_{i,u} \in D$ represents the correlation between the feature \mathcal{Q}_u and $\Omega_{i,u}$, $i = [1, \dots, |\Omega_u|]$, $D \in \mathbb{R}^{(H+W-1) \times W \times H}$.

After the above calculations, the obtained feature map is subjected to a Softmax operation to obtain an attention map A . The purpose of the Softmax operation is to normalize the position-related feature map, making the contribu-

tion of each position more clear. Finally, an aggregation operation is performed to obtain the long-range contextual information.

$$\mathcal{H}_{u'} = \sum_{i \in |\Phi_u|} \mathcal{A}_{i,u} \Phi_{i,u} + \mathcal{H}_u \quad (14)$$

where $\mathcal{H}_{u'}$ denotes the feature vector of the output feature map $\mathcal{H}' \in R^{C \times W \times H}$ at position u . $\mathcal{A}_{i,u}$ is a scalar value at channel i and position u . $\Phi_{i,u}$ denotes the set of feature vectors in V that are in the same row or column as channel i and position u .

3 Experiments and Results

3.1 Dataset and training details

Due to the lack of specific datasets for cine MR reconstruction, we validate the proposed method on two public cine MR datasets. The two datasets are ACDC [3] and SACMRI [1]. The automated cardiac diagnosis challenge (ACDC) dataset was created from real clinical exams acquired at the University Hospital of Dijon. The dataset consists of 150 exams (all from different patients), and the exams are divided into five categories, including normal case, heart failure with infarction, dilated cardiomyopathy, hypertrophic cardiomyopathy, and abnormal right ventricle. The short-axis cardiac MRI (SACMRI) dataset is provided by The Hospital for Sick Children in Toronto and consists of cardiac MR images obtained from 33 subjects.

We designed our model based on the machine learning framework PyTorch1.12.1 using Python3.8. In particular, we also use PyTorch-Lightning1.6.5, an efficient and convenient framework based on PyTorch. We trained the proposed model on a GPU server with an Intel Core i9-10900X CPU, two 10GB Nvidia RTX3080 GPUs, 32GB RAM, and 20GB VRAM. The batch size of the data is set based on the data size to ensure maximum memory utilization. The number of threads of the data reading program is 16. The initial learning rate is 1e-3. The learning rate dynamic adjustment strategy is ReduceLROnPlateau. The optimizer is AdamW [15]. The training epoch number is 100. Train with automatic mixed precision. The loss function used is the Mean Square Error (MSE) Loss (L2 Loss).

To evaluate the quality of the proposed method for cine MR image reconstruction, two commonly used image quality evaluation metrics were selected, namely the Structural Similarity Index (SSIM) [27] and Peak Signal-to-Noise Ratio (PSNR).

SSIM is based on the computations of luminance, contrast and structure terms between image x and y :

$$SSIM(x, y) = \frac{(2\mu_x\mu_y + c_1)(2\sigma_{xy} + c_2)}{(\mu_x^2 + \mu_y^2 + c_1)(\sigma_x^2 + \sigma_y^2 + c_2)} \quad (15)$$

where μ_x , μ_y , σ_x , σ_y and σ_{xy} are the local means, standard deviations, and cross-covariance for images x and y , respectively. $c_1 = (k_1 L)^2$ and $c_2 = (k_2 L)^2$, where L is the dynamic range of the pixel-values, $k_1 = 0.01$ and $k_2 = 0.03$.

Additionally, the performance of the model was measured statistically with PSNR. It is calculated via the MSE as:

$$\mathcal{PSNR} = 10 \lg \frac{\mathcal{R}^2}{\mathcal{MSE}} \quad (16)$$

where R is the maximum fluctuation in the input image.

3.2 Results and discussion

The quantitative comparison between the proposed method and other methods is shown in Table 1, 2. The first row shows the metrics for an undersampled image reconstructed directly from zero-padded k-space. The other two methods are kt FOCUSS [13] and DC-CNN [6], which are based on compressive sensing (CS) and deep learning, respectively. The proposed method outperformed other methods at three different k-space sampling rates (5%, 10%, and 30%). Particularly, at 5% k-space sampling rate or 20x acceleration, the proposed method showed excellent performance, with an SSIM improvement of 6.95% over DC-CNN and a PSNR decrease of 1.14 dB on SACMRI.

Table 1. Quantitative comparison on the SACMRI Dataset.

	30% k-space		10% k-space		5% k-space	
	PSNR (dB)	SSIM (%)	PSNR (dB)	SSIM (%)	PSNR (dB)	SSIM (%)
undersample	27.38	76.71	21.66	59.04	20.10	56.43
kt FOCUSS	30.79	88.72	24.05	71.98	22.73	68.29
DC-CNN	31.17	90.13	24.53	72.72	22.97	68.12
ours	31.95	90.63	25.45	77.73	24.11	75.07

Table 2. Quantitative comparison on the ACDC Dataset.

	30% k-space		10% k-space		5% k-space	
	PSNR (dB)	SSIM (%)	PSNR (dB)	SSIM (%)	PSNR (dB)	SSIM (%)
undersample	23.34	69.35	18.76	51.25	14.92	42.28
kt FOCUSS	27.96	85.01	21.64	69.61	18.54	59.30
DC-CNN	29.52	89.68	23.84	71.16	19.48	61.24
ours	30.82	90.76	24.17	72.02	21.06	64.06

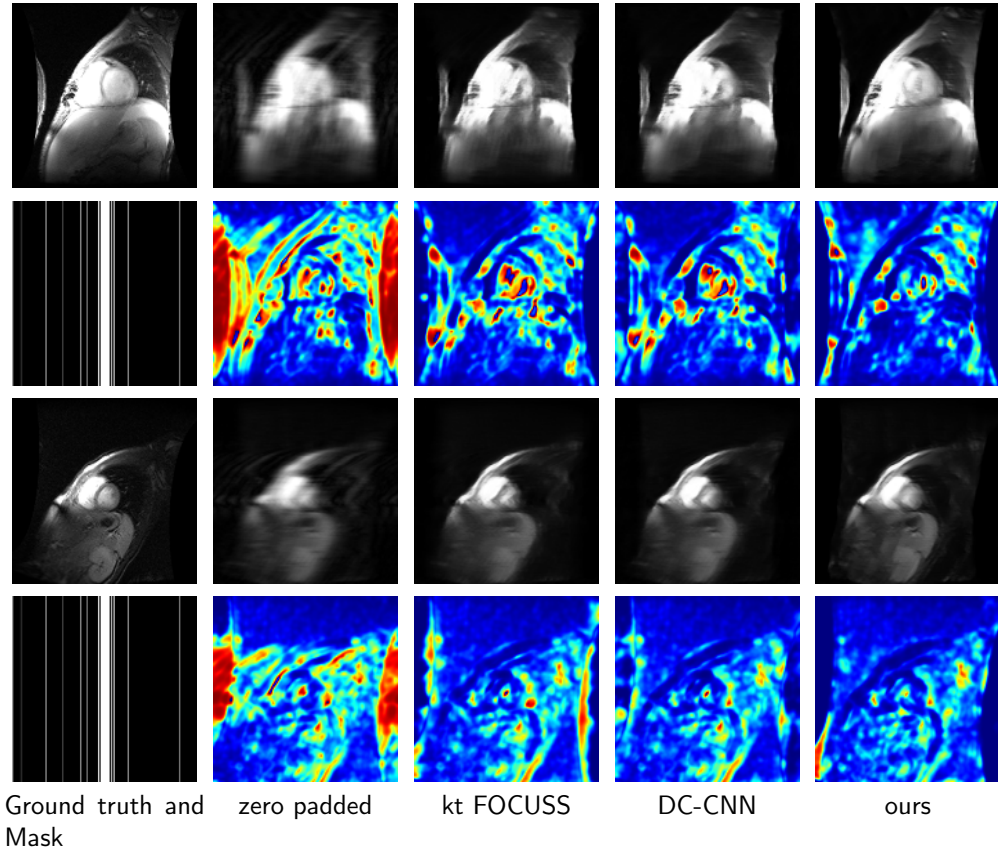


Fig. 4. The error between the image reconstructed by each method and Ground Truth at 10% k-space sampling rate.

We visualized the errors between the reconstructed images of each method and the Ground Truth in Fig. 4. and Fig. 5. It is evident that the CS-based method has stripe artifacts and significant reconstruction errors, and the deep learning-based DC-CNN still has large errors due to insufficient utilization of motion information. In contrast, our proposed method eliminates blurry artifacts and recovers more details.

The proposed method shows excellent performance, mainly due to the following three reasons: first, the motion-guided deformable alignment has strong exploration ability, which avoids the adverse effects of incorrect motion estimation on the model. Second, the second-order bidirectional propagation avoids the attenuation of aligned features over distant or future alignment, allowing the current frame to obtain additional spatial positional features during alignment. Third, attention mechanisms are introduced in both time and space to

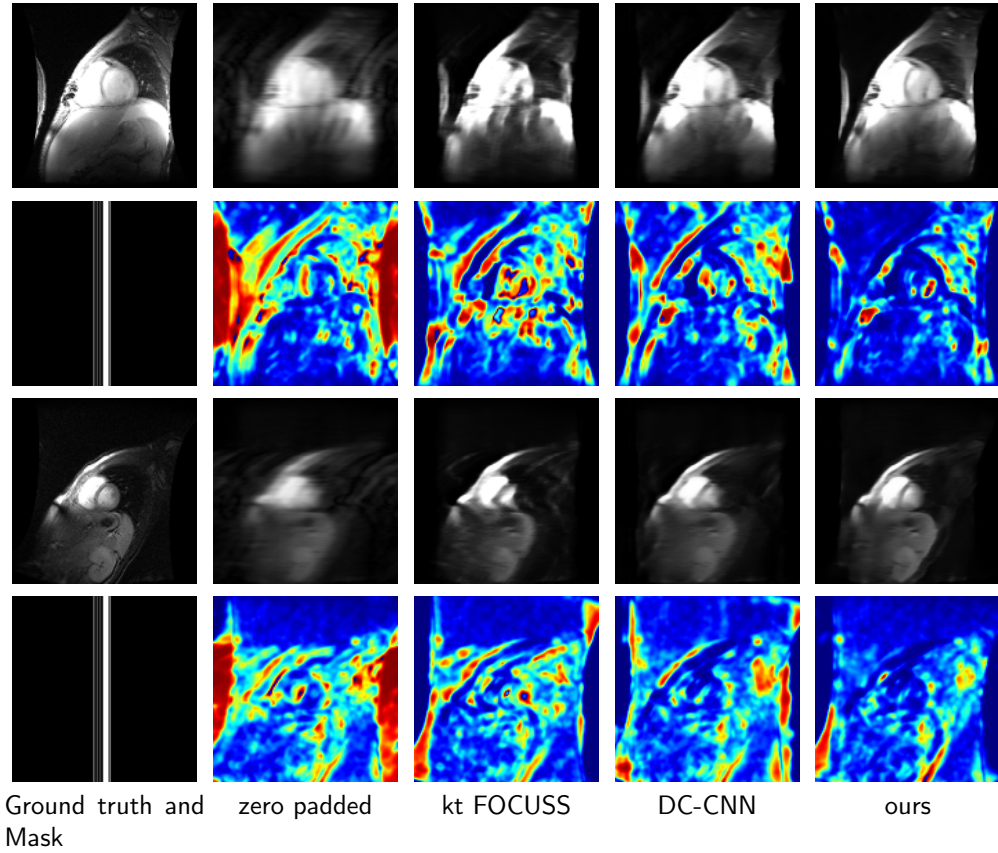


Fig. 5. The error between the image reconstructed by each method and Ground Truth at 5% k-space sampling rate.

ignore low-precision or inaccurate alignment and make the model more focused on useful information.

4 Conclusion

This paper proposes a motion-guided deformable alignment, second-order bidirectional propagation, and efficient spatiotemporal self-attention fusion-based model for movie magnetic resonance reconstruction. Experimental results show that the proposed method significantly improves the reconstruction effect of cardiac movie magnetic resonance at 5%, 10%, and 30% k-space sampling rates, and outperforms other advanced methods in terms of reconstruction performance. In the next step, we will apply the proposed method to cardiac magnetic resonance

reconstruction under free breathing, and further improve the reconstruction quality.

References

1. Andreopoulos, A., Tsotsos, J.K.: Efficient and generalizable statistical models of shape and appearance for analysis of cardiac mri. *Medical image analysis* **12**(3), 335–357 (2008)
2. Balachandrasekaran, A., Ongie, G., Jacob, M.: Accelerated dynamic mri using structured low rank matrix completion. In: *2016 IEEE International Conference on Image Processing (ICIP)*. pp. 1858–1862. IEEE (2016)
3. Bernard, O., Lalande, A., Zotti, C., Cervenansky, F., Yang, X., Heng, P.A., Cetin, I., Lekadir, K., Camara, O., Ballester, M.A.G., et al.: Deep learning techniques for automatic mri cardiac multi-structures segmentation and diagnosis: is the problem solved? *IEEE transactions on medical imaging* **37**(11), 2514–2525 (2018)
4. Chan, K.C., Wang, X., Yu, K., Dong, C., Loy, C.C.: Understanding deformable alignment in video super-resolution. In: *Proceedings of the AAAI conference on artificial intelligence*. vol. 35, pp. 973–981 (2021)
5. Chan, K.C., Zhou, S., Xu, X., Loy, C.C.: Basicvsr++: Improving video super-resolution with enhanced propagation and alignment. In: *Proceedings of the IEEE/CVF conference on computer vision and pattern recognition*. pp. 5972–5981 (2022)
6. Chlemper, J., Caballero, J., Hajnal, J., Price, A., Rueckert, D.: A deep cascade of convolutional neural networks for dynamic mr image reconstruction. *IEEE Transactions on Medical Imaging* **37**, 491–503 (2017)
7. Cole, E.K., Ong, F., Vasanaawala, S.S., Pauly, J.M.: Fast unsupervised mri reconstruction without fully-sampled ground truth data using generative adversarial networks. In: *Proceedings of the IEEE/CVF International Conference on Computer Vision*. pp. 3988–3997 (2021)
8. Dai, J., Qi, H., Xiong, Y., Li, Y., Zhang, G., Hu, H., Wei, Y.: Deformable convolutional networks. In: *Proceedings of the IEEE international conference on computer vision*. pp. 764–773 (2017)
9. Deshmane, A., Gulani, V., Griswold, M.A., Seiberlich, N.: Parallel mr imaging. *Journal of Magnetic Resonance Imaging* **36**(1), 55–72 (2012)
10. Han, Y., Sunwoo, L., Ye, J.C.: k-space deep learning for accelerated mri. *IEEE transactions on medical imaging* **39**(2), 377–386 (2019)
11. Huang, Q., Xian, Y., Yang, D., Qu, H., Yi, J., Wu, P., Metaxas, D.N.: Dynamic mri reconstruction with end-to-end motion-guided network. *Medical Image Analysis* **68**, 101901 (2021)
12. Huang, Z., Wang, X., Huang, L., Huang, C., Wei, Y., Liu, W.: Ccnet: Criss-cross attention for semantic segmentation. In: *Proceedings of the IEEE/CVF international conference on computer vision*. pp. 603–612 (2019)
13. Jung, H., Sung, K., Nayak, K.S., Kim, E.Y., Ye, J.C.: k-t focuss: a general compressed sensing framework for high resolution dynamic mri. *Magnetic Resonance in Medicine: An Official Journal of the International Society for Magnetic Resonance in Medicine* **61**(1), 103–116 (2009)
14. Lee, D., Yoo, J., Tak, S., Ye, J.C.: Deep residual learning for accelerated mri using magnitude and phase networks. *IEEE Transactions on Biomedical Engineering* **65**(9), 1985–1995 (2018)

15. Loshchilov, I., Hutter, F.: Fixing weight decay regularization in adam (2017)
16. Lustig, M., Donoho, D., Pauly, J.M.: Sparse mri: The application of compressed sensing for rapid mr imaging. *Magnetic Resonance in Medicine: An Official Journal of the International Society for Magnetic Resonance in Medicine* **58**(6), 1182–1195 (2007)
17. Patel, M.R., Klufas, R.A.: Gradient-and spin-echo mr imaging of the brain. *American Journal of Neuroradiology* **20**(7), 1381–1383 (1999)
18. Poddar, S., Jacob, M.: Dynamic mri using smoothness regularization on manifolds (storm). *IEEE transactions on medical imaging* **35**(4), 1106–1115 (2015)
19. Qin, C., Schlemper, J., Caballero, J., Price, A.N., Hajnal, J.V., Rueckert, D.: Convolutional recurrent neural networks for dynamic mr image reconstruction. *IEEE transactions on medical imaging* **38**(1), 280–290 (2018)
20. Ran, M., Hu, J., Chen, Y., Chen, H., Sun, H., Zhou, J., Zhang, Y.: Denoising of 3d magnetic resonance images using a residual encoder–decoder wasserstein generative adversarial network. *Medical image analysis* **55**, 165–180 (2019)
21. Sarasaen, C., Chatterjee, S., Bretkopf, M., Rose, G., Nürnberger, A., Speck, O.: Fine-tuning deep learning model parameters for improved super-resolution of dynamic mri with prior-knowledge. *Artificial Intelligence in Medicine* **121**, 102196 (2021)
22. Seegoolam, G., Schlemper, J., Qin, C., Price, A., Hajnal, J., Rueckert, D.: Exploiting motion for deep learning reconstruction of extremely-undersampled dynamic mri. In: *Medical Image Computing and Computer Assisted Intervention–MICCAI 2019: 22nd International Conference, Shenzhen, China, October 13–17, 2019, Proceedings, Part IV*. pp. 704–712. Springer (2019)
23. Tian, Y., Zhang, Y., Fu, Y., Xu, C.: Tdan: Temporally-deformable alignment network for video super-resolution. In: *Proceedings of the IEEE/CVF conference on computer vision and pattern recognition*. pp. 3360–3369 (2020)
24. Wang, S., Su, Z., Ying, L., Peng, X., Zhu, S., Liang, F., Feng, D., Liang, D.: Accelerating magnetic resonance imaging via deep learning. In: *2016 IEEE 13th international symposium on biomedical imaging (ISBI)*. pp. 514–517. IEEE (2016)
25. Wang, X., Girshick, R., Gupta, A., He, K.: Non-local neural networks. In: *Proceedings of the IEEE conference on computer vision and pattern recognition*. pp. 7794–7803 (2018)
26. Wang, X., Chan, K.C., Yu, K., Dong, C., Change Loy, C.: Edvr: Video restoration with enhanced deformable convolutional networks. In: *Proceedings of the IEEE/CVF Conference on Computer Vision and Pattern Recognition Workshops*. pp. 0–0 (2019)
27. Wang, Z., Bovik, A.C., Sheikh, H.R., Simoncelli, E.P.: Image quality assessment: from error visibility to structural similarity. *IEEE transactions on image processing* **13**(4), 600–612 (2004)
28. Wei, R., Chen, J., Liang, B., Chen, X., Men, K., Dai, J.: Real-time 3d mri reconstruction from cine-mri using unsupervised network in mri-guided radiotherapy for liver cancer. *Medical Physics* (2022)
29. Xiang, L., Chen, Y., Chang, W., Zhan, Y., Lin, W., Wang, Q., Shen, D.: Deep-learning-based multi-modal fusion for fast mr reconstruction. *IEEE Transactions on Biomedical Engineering* **66**(7), 2105–2114 (2018)
30. Yoo, J., Jin, K.H., Gupta, H., Yerly, J., Stuber, M., Unser, M.: Time-dependent deep image prior for dynamic mri. *IEEE Transactions on Medical Imaging* **40**(12), 3337–3348 (2021)
31. Zhu, B., Liu, J.Z., Cauley, S.F., Rosen, B.R., Rosen, M.S.: Image reconstruction by domain-transform manifold learning. *Nature* **555**(7697), 487–492 (2018)